Range segmentation for micro-Doppler of backscattered field by wind turbines

Medagli, Stefano; Krasnov, Oleg A.; Yarovoy, Alexander G.

DOI
10.23919/EuCAP.2017.7928323

Publication date
2017

Document Version
Final published version

Published in
11th European Conference on Antennas and Propagation, EuCap 2017

Range Segmentation for micro-Doppler of Backscattered Field by Wind Turbines

Stefano Medagli[1], Oleg A. Krasnov[2], Alexander G. Yarovoy[3]
Microwave Sensing, Systems and Signals (MS3)
Delft University of Technology, The Netherlands
[1]S.Medagli@tudelft.nl, [2]O.A.Krasnov@tudelft.nl, [3]A.Yarovoy@tudelft.nl

***Abstract*—In this paper, a simple electromagnetic model for wind turbine's backscattering is proposed. The wind turbine is modeled as a linear structure made of three rotating wires on which an electromagnetic fields impinges. Since a wind turbine is much bigger than typical radar range resolution cells, just a small part of it is involved in the backscattering for a single resolution cell. An analysis of the micro-Doppler features for each range cell involving the wind turbine is then proposed.**
The models are both compared and validated using real data acquired with PARSAX radar. The main features obtained from these models can be used to understand the backscattering mechanisms for a wind turbine and for developing of clutter mitigation algorithms.

***Index Terms*—radar; wind turbine; backscattering; micro-doppler; electromagnetic simulation;**

I. Introduction

Wind power industry is developing fast around the world. According to preliminary figures, the world has seen a new record in new wind installations, adding 63.690 MW within the year 2015. The total wind capacity of the world has reached 435 GW [1]. As wind power industry continuously grows, the number of wind farms is increasing and the dimension of wind turbine is becoming bigger and bigger in order to harvest more power. On the other hand, it is already well known that this kind of structures represent a serious problem for radar because of their strong Electromagnetic Interference (EMI), called Wind Turbine Clutter (WTC). The Radar Cross Section (RCS) of wind turbines dynamically changes and produces reflections with strong Doppler effect which decrease the efficiency of radars algorithm for moving target detection [2]. In many nations, rules concerning radar interference have caused planning of wind farms to be rejected or delayed [3]. Developing algorithms capable to mitigate WTC is a challenging research topic and one of the main task for radar community [4], [5].
In the following, a simplified model for WTC will be introduced. This model provides an analytical solution for the one already discussed in [6] and extends its scope to high resolution radar systems. This may be useful for testing mitigation algorithms and for better understanding backscattering mechanisms arising when a WT is being observed by radar systems.

The paper is organized as follows: Section II describes the EM model for WTC. Section III extends the model for high resolution radar systems. In Section IV, results obtained from real data by the S-band PARSAX radar for low and high resolution are shown in order to compare and validate the simulated results. In Section V conclusions are given.

II. Doppler spectrogram of a single rotating dipole for CW radar

Let's assume a spherical coordinate system and the dipole approximation for a windmill blade [6]. The center of rotation of the wind turbine is in the origin such that every point of a blade is in coordinates $(r', \theta', \phi' = 0)$ with $r' \in [0,\ L]$ and the radar receiver is in $(r, \theta, \phi = 0)$. The field radiated by a dipole with orientation along r' is

$$dE_\theta = j\eta k \frac{e^{-jkR}}{4\pi R} I_e(r'.\theta', \phi') sin(\theta - \theta') dr' \tag{1}$$

with I_e proportional to the incident wave ${E_\theta}^i$ such that

$$I_e(r', \theta', \phi') = {E_\theta}^i sin(\theta - \theta') e^{-jkR} \tag{2}$$

Using the far field approximation we have $R \approx r - r'cos(\psi)$ for the phase and $R \approx r$ for the amplitude, with $\psi = \theta - \theta'$, the equation (2) becomes

$$dE_\theta = j\eta k \frac{e^{-j2k\left(r - r'cos(\psi)\right)}}{4\pi r} I_e(r', \theta', \phi') sin^2(\psi)\ {E_\theta}^i(r)\ dr' \tag{3}$$

Integrating over the length of the blade\wire we obtain the field radiated as

$$E_\theta = jM \int_0^L e^{j2kr'cos(\psi)} dr' = jMg \tag{4}$$

$$\text{With} \qquad M = j\eta k \frac{e^{-2jkr}}{4\pi r} {E_\theta}^i(r) sin^2(\psi)$$

$$\text{and} \qquad g = \int_0^L e^{j2kr'cos(\psi)} dr' \tag{5}$$

It is important to remark that, since the blade is moving, we have

$$\theta' = \theta'(t) = \theta_0 + \Omega\ t \quad \Rightarrow \begin{cases} \psi = \psi(t) \\ M = M(t) \end{cases}$$

so, for a wind turbine blade we have

$$g = e^{jkLcos(\psi)} Lsinc\left(\frac{L}{\pi} kcos(\psi)\right) \tag{6}$$

978-88-907018-7-0/17/$31.00 ©2017 IEEE

Neglecting the term e^{-2jkr} in the formula (4), and making again explicit the time dependencies, the backscattered field becomes

$$E_\theta = j\eta k \frac{1}{4\pi r} {E_\theta}^i(r) sin^2(\psi(t)) \\ e^{jkLcos(\psi(t))} Lsinc\left(\frac{L}{\pi} kcos(\psi(t))\right) \quad (7)$$

with amplitude and phase.

$$|E_\theta| = \eta k \frac{1}{4\pi r} {E_\theta}^i(r) sin^2(\psi(t)) \, Lsinc\left(\frac{L}{\pi} kcos(\psi(t))\right) \quad (8a)$$

$$\angle E_\theta = \Phi(t) = kLcos(\psi(t)) \quad (8b)$$

The instantaneous Doppler frequency so can be evaluated as

$$f_d(t) = \frac{d\Phi}{dt} = kL\Omega sin(\psi(t)) \quad (9)$$

From the two formulas (8a)-(9) it is easy to recognize that when the direction of the blade and the LOS of the radar are perpendicular, so $\psi = \frac{\pi}{2} + n\pi$, the doppler frequency and the amplitude have their maximum value. On the other hand, we can derive that when the blade is positioned along the LOS of the radar ($\psi = n\pi$) we will have a null for the doppler frequency and also for the amplitude.
The magnitude of the backscattered field variates with time and its maximum value and variationis is related to the length of the blade L. Doppler frequency variates with time too and its variation and maximum value depend on the length of the blade L and its rotational rate Ω.

A. Simulated examples

The following results simulate the spectrograms for a S-band radar ($f = 3\ Ghz$) observing a wind turbine from a side, with PRF $1\ kHz$. The aspect angle θ is $90°$. The Short Time Fourier Transform is obtained using rectangular windows for 128 samples with 99% of overlapping. In Figure 1 is is shown the spectrogram obtained considering one full rotation of a single rotating dipole with length $L = 100\lambda = 10m$, period $\Omega = 6\ rpm$. The vertical axes (the slow time dimension) is not an actual time but is the angle $\theta'(t) = \Omega_{dgps} t$. Anyway the correspondence is bijective.
Using this representation is easier to recognize geometrical features of the dipole while rotating; e. g. we can see the maximum value for amplitude and doppler frequency in $\theta' = 0°$ and $180°$ (i. e. $\psi = \pm 90°$). We can also see that after this perpendicular position of the blade (with respect to the LOS of the target), the amplitude becomes fainter and the Doppler frequency decrease with a "sin-like" trend. Both go to zero when $\theta' = 90°$ and $270°$. At the same time, during the rotation, we can appreciate variations of the Zero-Doppler component.

Commonly, horizontal wind turbines are made of three equispaced blades rotating with the same center of rotation. Using this assumption and evaluating the field from 3 dipoles with angular distance equal to $120°$ we obtain the spectrogram

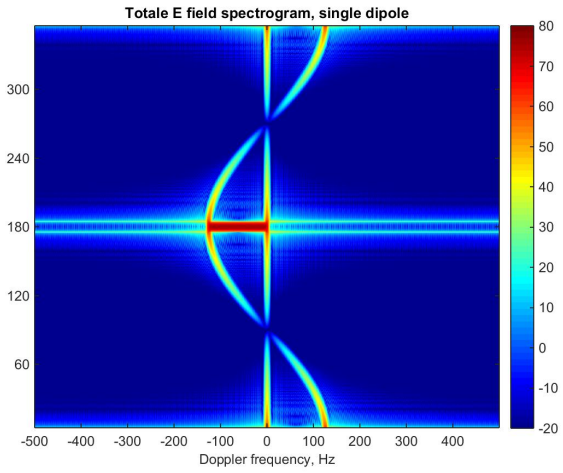

Figure 1. Spectrogram of the field evaluated for a single rotating blade obtained from simulated data.

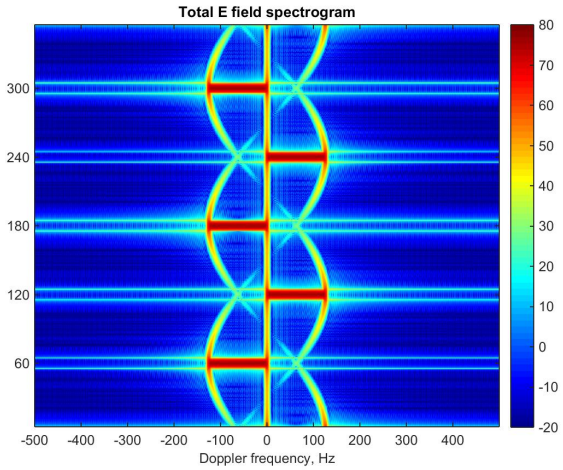

Figure 2. Spectrogram of the field evaluated for 3 rotating blades obtained from simulated data.

shown in Figure 2. It is worth noticing that this model does not take into account any coupling\multi-bounce effect between the blades and totally neglects the mast.

III. High Resolution Radar: Range Bin Analysis

Actually a wind turbine is an object that has great extension not only compared to the typical wavelength of radar systems but also compared to the extension of a range resolution cell $\Delta r = c/2B$. Due to this reason, for a sufficiently long time on target, a wind turbine blade migrates from a range gate to another. It is interesting to observe what happens in each range cell while the blades are moving. First, will be simulated what happens when just one blade\dipole moves and then the model will be extended to a three bladed structure.
In the following example we considered the simplified geometry shown in Figure 3 in which what we call range cell 0, is the range cell in which the center of rotation of the blade(s) is. Center of symmetry of this cell is the center of rotation

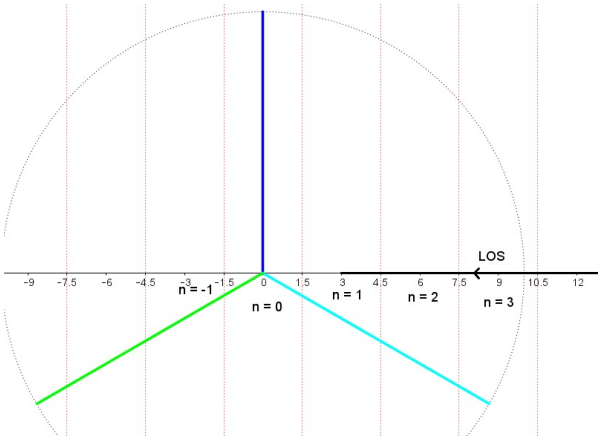

Figure 3. An example of the geometry of the range gates.

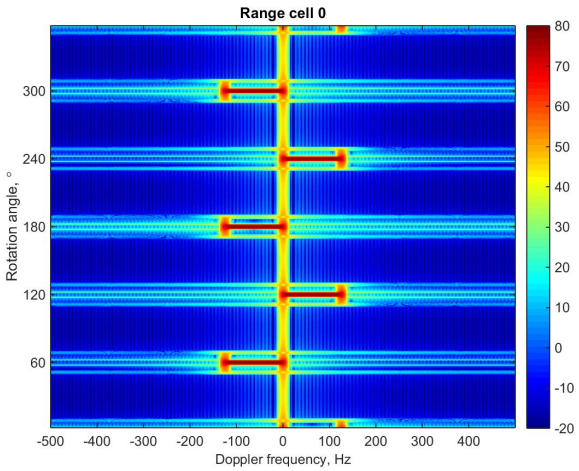

Figure 4. Spectrogram for range cell 0 obtained from simulated data.

of the blade, that is also the origin of our coordinate system. So, for a radar placed in $\theta = 90°$, whose LOS is parallel to the x axes we have that range cell 0 involves any point with $|x| \leq \frac{\Delta r}{2}$. Then, moving toward the radar, there will be range cells identified with a positive number, moving in opposite direction on the x axes there will be the negative ones. Generalizing, we will have that the n-th cell goes from ${x'}_n$ to ${x''}_n$ with

$${x'}_n = (2n-1)\frac{\Delta r}{2} \tag{10a}$$

$${x''}_n = (2n+1)\frac{\Delta r}{2} \tag{10b}$$

In table I an example that takes into account five range cells with a given range resolution $\Delta r = 3m$, may clarify this concept.

Table I
RANGE BIN CRITERIA FOR RANGE RESOLUTION $\Delta r = 3m$.

Cell nr. [n]	From [m] $(2n-1)\frac{\Delta r}{2}$	To [m] $(2n+1)\frac{\Delta r}{2}$
-2	- 7.5	- 4.5
-1	- 4.5	- 1.5
0	- 1.5	+ 1.5
1	+ 1.5	+ 4.5
2	+ 4.5	+ 7.5

While a blade is rotating, his projection on the radar LOS continuously change his length, following the *cosine* of the angle between the blade and the radar LOS.

$$L_{LOS} = L \cdot \ cos(\theta - \theta'(t)) = L \cdot \ cos(\psi(t)) \tag{11}$$

With this assumption we can easily recognize that for each range cell but the 0-th, we will see at most the tip of the blade, but not his center of rotation. On the other hand, for the 0-th one, we will see the center of rotation of the blade for most of the time and, just in some time sample, also the tip of the blade. Thus, we distinguish between two different cases

1) Only the center of rotation of the blade is in the range cell;
2) Only the tip of the blade is in the range cell;

The result obtained in (6) considers both the tip and the center of rotation of the blade, in the same range cell at the same time, so we must slightly modify it to take into account this two cases. In the first case, the result of the integral in formula (5) becomes:

$$g = -j \ \frac{1}{2kcos(\psi(t))} \tag{12}$$

For the second case we have that the results of the integral in (5) becomes

$$g = -j \ \frac{e^{j2Lkcos(\psi(t))}}{2 \ kcos(\psi(t))} \tag{13}$$

This time we have a phase term that gives the same instantaneous Doppler frequency obtained in formula (9).

A. Simulated examples

Knowing in which range cell the blade will appear for each time samples, a spectrogram for each range cell can be derived. The Figures from 5 to 6 show the spectrogram for some of the positive numbered range cells and are obtained considering a three rotating dipoles with length $L = 100\lambda = 10m$, rotation frequency $\Omega = 6 \ rpm$ and resolution cell $\Delta r = 3 \ m$. Again, for the vertical axes, instead of a time, it is reported the angle of rotation of the first blade $\theta(t) = \Omega_{dgps} \ t$. The radar parameters are the same used in section II-A.

In Figure 4 we can see that the presence of a wind turbine induces periodical oscillation for the Zero-Doppler component in correspondence of the flashes arising when a blade is orthogonal to the LOS of the radar.

Also in Figures 5 and 6, other fainter flashes, involving all the frequencies, are visible when the blade migrates from a range cell to another.

For each range cell, we can see a "symmetricity" in the behavior of the spectrogram: in the same range cell, first the blade moves toward the radar, having so a positive Doppler,

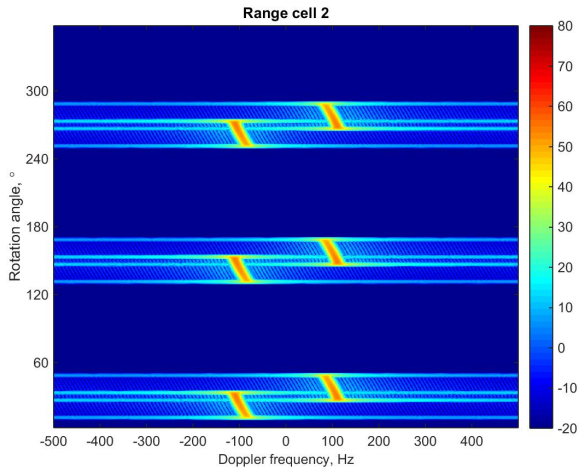

Figure 5. Spectrogram for the range bin 2 obtained from simulated data.

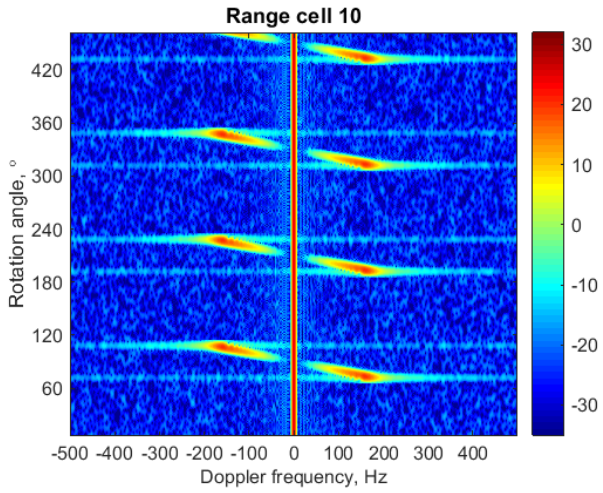

Figure 6. Spectrogram for the range bin 3 obtained from simulated data. In this representation, it has been added an AWGN noise and a Zero-Doppler component.

then, when the rotation angle $\theta' = 90°$, the velocity over the LOS becomes 0 and then changes sign and the blade starts moving away from the radar, having so a negative Doppler.
The higher is the order of the range cell, the longer is the angle\time interval during which the blade is in the cell. It may also happen that more then one blade's tip is in the same range cell in the same time sample (Figure 5).

IV. Real data from PARSAX radar

A. Low resolution measurements

The theoretical results described above simulates the return for a S-band radar ($f = 3\ Ghz$) observing a wind turbine from a side, with PRF $1\ kHz$ for one full rotation period of the wind turbine. The Short Time Fourier Transform was obtained using rectangular windows for 128 samples with 127 overlapping samples.
In Figure 7 is shown the spectrogram obtained from real measurements obtained from the PARSAX radar developed at TU Delft [7], [8]. This is an S-band polarimetric Doppler FMCW research radar that is highly reconfigurable, having ability to change the bandwidth of transmitted signals (and consequently, the range resolution) within very wide interval (from 3 to hundreds meters). Wind turbine under observation is a Vestas V66 type with blade length $32\ m$ and rotational rate was visually verified at the time of the measurements as around $9\ rpm$. The spectrogram has been calculated based on the radar data, which were measured with sweep repetition frequency $1\ kHz$ and frequency bandwidth $1.5\ MHz$ (range resolution $100\ m$). It is immediately visible that the spectrum is folded because of the limited PRF and the high velocity of the wind turbine. Spectrogram confirms the flashes when the angle $\theta = 0$ or $180°$. Flashes have a "modulation" such that not all the frequencies have the same amplitude, this is maybe due to constructive and destructive interaction between the backscattered fields from each point of the blade. Unfolding the spectrogram, we can see that the tip of the blade has much stronger backscattering for positive velocities. In the black rectangle it is enlightened the "sin-like" trend of the frequency, already discussed in the theoretical model. The time to have three flashes (one full rotation) is around $6.6\ s$, that confirms that the rotational rate is about $9.1\ rpm$.
A new feature that could not be found in the theoretical model, is a slanted Doppler component appearing in between two flashes due to one of the other two blades close to horizontal position. It appears first as a negative velocity, then, when the blade is parallel to the LOS of the radar, it crosses 0 and then again becomes positive. This feature shows an acceleration of around $3g$, so abrupt to suggest a relation with some hidden EM mechanism, rather than a real mechanical movement.

In Figure 8, in blue, it is shown the Zero-Doppler profile of the backscattered signal in slow time. As expected, due to the movement of the blades, the Zero-Doppler profile has a regular trend, with excursions of around 3% from the maximum ($2-3\ dB$), related to the periodicity of the rotation of the blades. Superimposed, in red and green, are shown the profiles for for two other components (195 and $-195\ Hz$) that appear during the flashes, when the blades are orthogonal to the LOS. It is clearly visible that the peaks of the Zero-Doppler come immediately after the flashes occurring for the positive frequencies and before the ones for the negative ones. This may be related to a shadowing effect of the mast (or of some other stationary clutter) operated by the blades.

B. High resolution measurements

In figure Figure 9 is shown another spectrogram for the same wind turbine. This time, the frequency bandwidth was set to $50\ MHz$, such that the range resolution was $\Delta\ r = 3.3\ m$. The spectrogram confirms a "sin-like" trend and the appearance of flashes when a blade is migrating from a range cell to another one. In the same Figure we can see that rotation of the blade still describes a sinusoidal Doppler, even after the range migration, but with a much fainter magnitude. This effect could not be seen in the simulated data in Figure 6

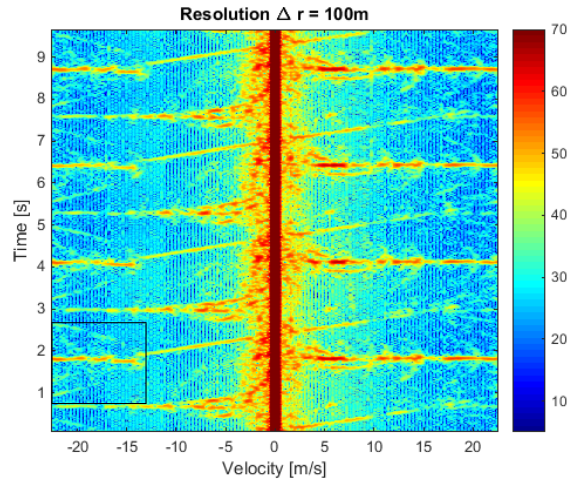

Figure 7. Spectrogram obtained from PARSAX measurements with resolution $\Delta r = 100\ m$.

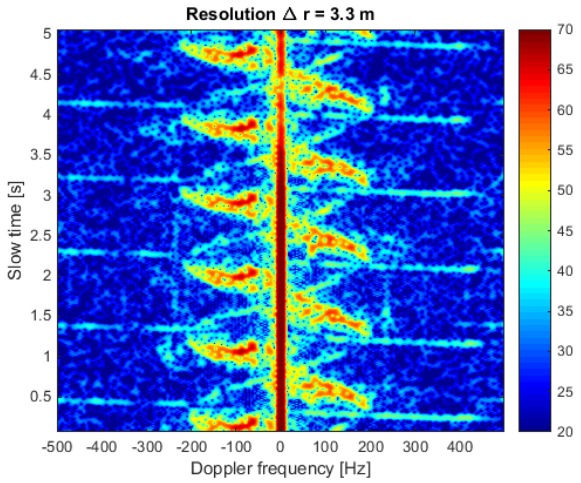

Figure 9. Spectrogram obtained from PARSAX measurements with resolution $\Delta r = 3.3\ m$.

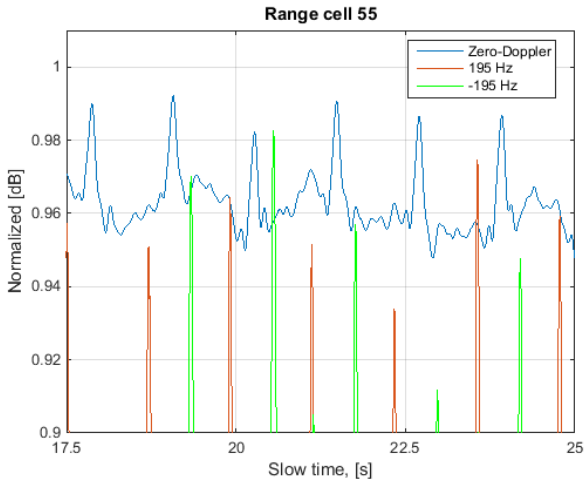

Figure 8. Zero-Doppler, 195 Hz and $-195\ Hz$ profiles vs. slow time. Since the two other frequencies have magnitude about 30 dB lower than the Zero-Doppler, each plot has been normalized to their maximum value, in order to show their fluctuations in a bigger scale.

because the model does not take into account the influence of nearby range cells.

V. Conclusion

In this paper, we used a simplified EM model to describe a wind turbine Doppler temporal pattern. The model does not take into account coupling\multi-bounce effects between the blades or the blades and the mast, but still gives a good first approximation of the micro-Doppler signature of the signal backscattered by a wind turbine. The model describes how parameters such as blades' length L, angular speed Ω and reciprocal positioning between blades and radar ψ, influence micro-Doppler signature of a wind turbine.

A pattern for the Zero-Doppler component of WTC has been found and compared with the trends for frequencies appearing during a "flash".

Given the dimension of the target, much bigger than the range resolution of a radar system, an analysis of the expected backscattering from each range cell involving the target, has been proposed. This new analysis enlightened the appearance of new, fainter flashes in the spectrogram, related to the range migration of the target.

Simulated data have been compared with real measurements operated by means of PARSAX radar.

VI. Acknowledgment

The authors would like to thank Fred van der Zwan and Etienne Goossens for their support in the PARSAX radar maintenance and data collection during the experiment.

References

[1] World Wind Energy Association, "The World sets New Wind Installations Record: 63,7 GW New Capacity in 2015," 2016. [Online]. Available: http://www.wwindea.org/the-world-sets-new-wind-installations-record-637-gw-new-capacity-in-2015/

[2] O. A. Krasnov and A. G. Yarovoy, "Polarimetric micro-Doppler characterization of wind turbines," in *2016 10th European Conference on Antennas and Propagation, EuCAP 2016*, Davos, Switzerland, 2016, p. 5.

[3] L. Rashid and A. Brown, "Partial treatment of wind turbine blades with radar absorbing materials (RAM) for RCS reduction," *Antennas and Propagation (EuCAP), 2010 Proceedings of the Fourth European Conference on*, 2010.

[4] R. R. Ohs, G. J. Skidmore, and G. Bedrosian, "Modeling the Effects of Wind Turbines on Radar Returns," no. 1, pp. 272–276, 2010.

[5] J. Perry and A. Biss, "Wind farm clutter mitigation in air surveillance radar," *Ieee Aerospace and Electronic Systems Magazine*, vol. 22, no. 7, pp. 35–40, 2007.

[6] O. A. Krasnov and A. G. Yarovoy, "Radar micro-doppler of wind-turbines: Simulation and analysis using slowly rotating linear wired constructions," *International Journal of Microwave and Wireless Technologies*, vol. 7, no. 3-4, pp. 459–467, 2015.

[7] O. Krasnov, G. Babur, L. Ligthart, and F. V. D. Zwan, "Basics and first experiments demonstrating isolation improvements in the agile polarimetric FM-CW radar - PARSAX," *International Journal of Microwave and Wireless Technologies*, vol. 2, no. 3-4, pp. 419–428, 2010. [Online]. Available: http://www.journals.cambridge.org/abstract_S1759078710000371

[8] O. Krasnov, L. Ligthart, Z. L. Z. Li, P. Lys, and F. V. D. Zwan, "The PARSAX - full polarimetric FMCW radar with dual-orthogonal signals," *2008 European Radar Conference*, no. October, pp. 84–87, 2008.